

Scintillation light simulation in big-sized BaF₂ and pure CsI crystals.

Z. Usubov

Joint Institute for Nuclear Research, Dubna, Russia

April 5, 2016

Abstract

We have investigated scintillation light distribution in BaF₂ and pure CsI crystals with dimensions 3x3x20 cm³ using the Geant4 toolkit. The diffuse wrapping material is selected as coating for the crystals. The simulated cosmic muons and 105 MeV electrons are used as beam particles. The optical attenuation along the crystals is explored with the simulation data. We have demonstrated the impact of the crystal surface finish on the light distribution at the crystal end, optical photon arrival time, incidence angle distributions, and optical attenuation for the studied crystals.

1 Introduction

Flavor changing by all neutral current interactions is strongly suppressed in the Standard Model. The new physics scenarios - supersymmetry, extra dimensions, little Higgs, quark compositeness - naturally allow and predict the charged lepton flavor violation at some level (see, e.g.,[1]).

The aim of the $\mu \rightarrow e$ conversion experiments is to search for the coherent conversion of the muons from muonic atoms to the electrons in the field of a nucleus through some new lepton flavor violation interactions. The conceptual designs[2, 3] of the $\mu \rightarrow e$ conversion experiments include a calorimeter able to measure the energy of the electrons with the resolution $<5\%$ for 105 MeV and the time resolution ~ 1 ns to provide the trigger signal and measure track positions in addition to the tracking chambers. The calorimeter will consist of the $\sim 3 \times 3$ cm² dense crystals and are >10 radiation lengths long.

In this paper we present the results of the Geant4 Monte Carlo simulation of the optical processes in square cross section BaF₂[4] and CsI[5] crystals. Both of these crystals are considered as candidates for the electromagnetic calorimeter of the Mu2e experiment. The next section briefly describes the strategy of simulating optical photons in a crystal using the Geant4 toolkit. The properties of the crystals, choice of the optical model, and

Crystal	NaI(Tl)	CsI(pure)	BaF ₂
Density (g/cm ³)	3.67	4.51	4.89
Melting Point (°C)	651	621	1280
Radiation Length (cm)	2.59	1.86	2.03
Molière Radius (cm)	4.13	3.57	3.10
Interaction Length (cm)	42.9	39.3	30.7
Refractive Index	1.85	1.95	1.50
Hygroscopicity	Yes	Slight	No
Luminescence (nm)(at peak)	410	420(310)	300(220)
Decay Time (ns)	245	30(6)	650(0.6-0.8)
Light Yield(Brightness)(%)	100	3.6(1.1)	36.0(4.10)
d(LY)/dT(%/°C)	-0.2	-1.4	-1.9(0.1)

Table 1: Useful characteristics[11] of dense crystals as a Mu2e calorimeter material. The values correspond to the slow or fast(in parentheses) scintillation component.

crystal surface finish are described. In Section 3 we give the optical photon simulation results. We have examined the photon distributions at the end of the BaF₂ and CsI crystals. Optical attenuation along the crystals was studied. The photon arrival time and the incidence angle were estimated. We compared the simulation data with the polished and unpolished crystal surfaces. We end with a short conclusion in Section 4.

2 Some features of scintillating crystal modeling

Monte Carlo simulations play a crucial role in determining the optimal crystal material and suitable calorimeter design. The Geant4 code takes into account optical properties of materials and is a reliable tool for studying a large class of scintillators.

Two types of photons are involved in scintillation processes in crystals: high energy photons (e.g., 511 keV annihilation photons from the ²²Na or ⁶⁸Ge/⁶⁸Ga, 662 keV photons from the ¹³⁷Cs radioactive source, etc.) and low-energy optical photons (photons with a wavelength much greater than the typical atomic spacing). The optical photons further undergo the following processes: bulk absorption, Rayleigh scattering, reflection and refraction at medium boundaries, and wavelength shifting. The boundary processes on all crystal surfaces play an important role in tracing photons in crystals. Compared with them, photon self-absorption is less significant[6].

In Geant4[7] scintillator surfaces follow the GLISUR (was realized earlier for Geant3.21[8]), LUT (look-up-tables)[9] or UNIFIED[10] models. The LUT model is based on measur-

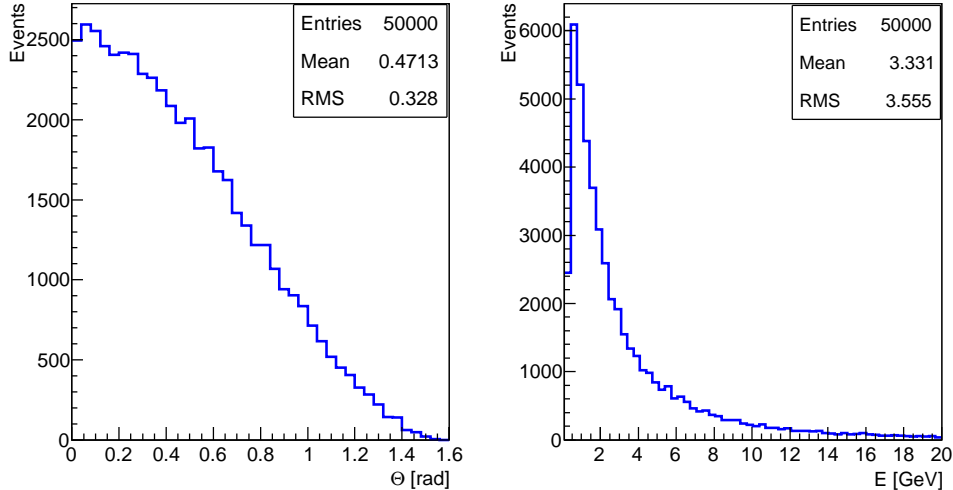


Figure 1: The azimuthal angular distribution (left panel) and energy spectrum (right panel) of cosmic muons as simulated according to[12].

ing the angular reflectivity distribution inside crystal and has been realized only for $\text{Bi}_4\text{Ge}_3\text{O}_{12}$ (BGO) crystals as yet. The criterion for BGO crystal size selection in these measurements is that the largest surface length must be smaller than 50 mm. This is an excellent way to model light transportation and boundary effects in crystals, but it is not applicable to our simulation.

In the UNIFIED model the surfaces are made up of micro-facets with normal vectors that are oriented around the average surfaces according to the Gaussian distribution with mean 0 and standard deviation given by a user-adjustable value and known as σ_α . The magnitude of this deviation determines whether the surface is polished, etched, or ground and is set to 1.3° , 3.8° , and 12° , respectively. These options of crystal surface are combined with different coating conditions. In this simulation we use the UNIFIED model for the processes between two dielectric materials (surface type was set to dielectric-dielectric). We combined the polished and ground surface finishes with the frontpainted crystal wrapping option, which implies the absence of an air gap between the crystal and the wrapping and represents diffuse (Lambertian) reflection.

To simulate the whole process in the scintillators, the physics list included low-energy electromagnetic physics and scintillation and transportation of optical photons. The index of refraction and the fast and slow components of the scintillation photon distributions for BaF_2 and CsI as a function of the wavelength were used. The scintillation photons are generated as a pure Poisson process (RESOLUTIONSCALE parameter was

set to 1). The brightness of the crystal is important for the energy and timing resolution of the calorimeter. The corresponding number of scintillation photons was calculated in this analysis assuming that brightness of BaF₂ and CsI is 11.8 photons/keV and 2.8 photons/keV, respectively. The Birk's kB' constant was taken to be 0.00368 mm/MeV and 0.00152 mm/MeV for BaF₂ and CsI, respectively. The relative strength of the fast component as a fraction of total scintillation yield is given by the YIELDRATIO. This variable values 15% for BaF₂ and 80% for CsI was used in simulation. The simulation results for effective decay time was determined to be 638.8 ns and 12.5 ns respectively for BaF₂ and CsI crystals.

3 Simulation and results

This simulation was performed using Geant4.10.0 for inorganic scintillators BaF₂ and pure CsI with the dimensions 3x3x20 cm³. The properties of these crystals[11] are compared with NaI(Tl) in Table 1. We also note that BaF₂ is the fastest scintillator now and pure CsI is quite soft and one of the cheapest crystals. For both crystals all surfaces are polished or ground. We collected photons from one of the crystal ends (3x3 cm²) (hereinafter referred to as photodetector side). On the photodetector side of the crystal photons are fully absorbed. All other surfaces were wrapped in a highly reflective (R=98%) diffuse coating without an air gap.

Cosmic muons were generated according to[12] in the range 0.3-5000 GeV and injected always perpendicular to the 3x20 cm² crystal surface. The azimuthal angular distribution and energy spectrum of the simulated cosmic muons are shown in Figure 1.

Figures 2 and 3 show the XY position-dependent number of optical photons as seen by the photodetector side of the polished and ground BaF₂ and CsI crystals. The 5000 cosmic muons impinge perpendicularly on the crystal lateral surface in -Y direction at different distance *l* from the photodetector side along the crystal Z-axis. Scintillation occurs at various Z positions in a crystal. It can be seen that if the muon impinging point is close to the crystal photodetector side, the photon distribution for the polished crystal is not uniform and smoothed with increasing *l*. These figures illustrate the difference of the light distribution for two crystals. The ground surface of the crystal leads to the focusing of the light on the center of the crystal photodetector side. On the other hand, if the surface is polished, significantly more photons reach the end of the crystals.

Figures 4 and 5 plot the mean values and standard deviations of the fit with the Gaussian function of the optical photon distributions on the photodetector side as a function of the beam impinging position, actually the position of the deposited energy inside the crystal. The simulated data correspond to the CsI (left panel) and BaF₂ (right panel) crystals.

As expected, the effective attenuation length λ_{eff} decreases when the crystal faces

are roughened. This is because some photons leave the crystal instead of being totally reflected. The path of the photons will be significantly changed. Note that the total bulk attenuation length λ_{eff} , absorption attenuation length λ_{ab} , and scattering attenuation length λ_s are related as

$$\frac{1}{\lambda_{eff}} = \frac{1}{\lambda_{ab}} + \frac{1}{\lambda_s}.$$

As shown in the figures significant light loss is caused by the unpolished crystal surface. With the BaF₂ crystal, more photons appears to be collected according to the higher brightness of crystal.

Figure 6 show the XY position-dependent optical photons at the photodetector side of the polished and ground BaF₂ and CsI crystals when 2000 electrons with E=105 MeV impinge on the center of the opposite side along the Z-axis. It can be clearly seen that the distributions are uniform for the polished crystal surfaces. The photons are more focused on the center of the photodetector side if the crystal surface is ground. These distributions have the same behavior as in the case of cosmic muons impinging on the crystals. The corresponding number of photon distributions is shown in Figure 7. The results of the Gaussian fit are also shown in figure. The decrease the number of optical photons due to the surface roughening is ~ 4.8 and ~ 4.1 times for BaF₂ and CsI, respectively.

We note that the energy depositions in the 3x3x20 cm³ crystals when 105 MeV electrons impinge perpendicularly on the center of the 3x3 cm² side is 73.96 ± 0.06 MeV and 70.33 ± 0.06 MeV for BaF₂ and CsI, respectively.

The photon arrival time is important for the time resolution of the detector[13]. The dependence of the photon arrival time on the distance of the traversing muon to the photodetector side is shown in Figure 8 for the BaF₂ crystal with the ground and polished surfaces. It is seen that for the polished crystal (right column) the distributions have two peaks. The photons which travel directly to the photodetector side without undergoing any optical interaction give the first peak. The photons that are reflected from the opposite end of the crystal and arrive at the photodetector side without any other reflections give the second peak. The peak positions correspond to the distance from the beam impinging point to the photodetector side. The second peak amplitude increases rapidly with decreasing distance from the beam impinging point to the opposite side. In contrast, for the crystal with the ground surface only the peak from the photons impinging on the photodetector side without any previous reflections is clearly seen. Again, the peak position corresponds to the beam impinging point. In this case the "indirect" photons (which undergo reflection from the lateral sides) lead to the broadening of the distribution with increasing distance to the photodetector side.

Figure 9 demonstrates the arrival time and Figure 10 the incidence angle (the angle with respect to the crystal Z-axis) distribution for optical photons at the photodetector

side for the polished and ground BaF₂ and CsI crystals. The electrons with E=105 MeV impinge on the center of the opposite side. In Figure 10, -1 on X-axis corresponds to the normal incidence of photons. The ratios of the mean photon arrival time in the CsI crystal to the mean photon arrival time in the BaF₂ crystal for the polished and ground surfaces are 1.8 and 2.1, respectively. Note that the ratio between the refraction indices of CsI and BaF₂ is 1.3. This simulation shows that the polished and ground crystal surfaces lead to different optical photon angular distributions. The number of photons depends strongly on the incidence angle.

4 Conclusion

We presented the results of the Geant4 simulation of the optical photon transport and surfaces border effects in the 3x3x20 cm³ BaF₂ and pure CsI crystals. Cosmic muons and electrons with E=105 MeV were used as beam particles. The effect of surface roughening on scintillation light was studied in crystals with diffuse wrapping.

We found that the crystal surface finish plays a crucial role in the spatial distribution and absolute value of optical photons in scintillating crystals. The simulation studies showed that in the crystals with the unpolished surface the effective attenuation length decreases and hence polished crystals make it possible to collect significantly more photons. However, the ground crystal surface gives more light focused on the center of the crystal end.

The photon arrival time at the crystal photodetector side was explored as a function of the cosmic muon traversing position and the crystal surface treatment. The impact of the crystal surface finish on the optical photon incidence angle was also demonstrated.

We gratefully acknowledge the very helpful discussions and suggestions by Y. Budagov, Y. Davydov, V. Glagolev and P. Murat.

References

- [1] J. Hisano and D. Nomura, Phys. Rev. D59, (1999) 116005;
K. Agashe, A.E. Blechman and F. Petriello, Phys.Rev. D74, (2006) 053011;
M. Blanke et al., JHEP 0705, (2007) 013.
- [2] K. Akhmetshin et al., Letter of Intend for Phase-I of the COMET Experiment at J-PARC, KEK/J-PARC-PAC 2011-27, March 11, 2012.
- [3] L. Bartoszek et al., Mu2e Technical Design Report, FERMILAB-TM-2594, FERMILAB-DESIGN-2014-01, arXiv:1501.05241[physics.ins-det].

- [4] A.R. Gabler et al., Nucl.Instrum.Meth. A346, (1994) 168-176;
R-Y. Zhu, Nucl.Instrum.Meth. A340, (1994) 442-457;
G. Mukherjee et al., EPJ Web of Conferences 66, (2014) 11026.
- [5] Z-Y. Wei and R-Y. Zhu, Nucl.Instrum.Meth. A326, (1993) 508-512;
E. Frlež et al., Nucl.Instrum.Meth. A459, (2001) 426-439;
C. Amsler et al., Nucl.Instrum.Meth. A480, (2002) 494-500;
KTeV Collaboration (P.N. Shanahan for collaboration), The performance of a new CsI calorimeter for the KTeV experiment at Fermilab, Frascati Phys.Ser. 6, (1996) 717-726.
- [6] G.F. Knoll, Radiation detection and measurement, Third Edition, John Wiley and Sons, Inc., Ann Arbor, 2000, pp. 247-248.
- [7] S. Agostinelli et al., Geant4 - a simulation toolkit, Nucl.Instrum.Meth. A506, (2003) 250-303.
- [8] Geant - Detector Description and Simulation Tool, CERN Program Library Long Writeup W5013, CERN, Geneva 1993.
- [9] M. Janecek and W.W. Moses, Simulating Scintillator Light Collection Using Measured Optical Reflectance, IEEE Transactions on Nuclear Science, v.57, no.3, (2010) 964.
- [10] S.K. Nayar, K. Ikeuchi and T. Kanade, Surface reflection: Physical and geometrical perspectives, IEEE Transactions On Pattern Analysis And Machine Inteligence, 1991, 13, 611;
A. Levin and C. Moisan, A more physical approach to model the surface treatment of scintillation counters abd its implementation into DETECT, IEEE Nucl. Sci.Symp. Conf. Rec. 2, (1996), 702.
- [11] R. Mao, L. Zhang, R-Y. Zhu, IEEE Transactions on Nuclear Science, v.55, no.4, (2008) 2425.
- [12] L.N. Volkova, G.T. Zatsepin, L.A. Kuzmichev, Yad.Fiz. 29, (1979) 1252, Sov.J.Nucl.Phys 29, (1979) 645.
- [13] R-Y. Zhu, The Next Generation of Crystal Detectors, arXiv:1308.4937[physics.ins-det];
V.Ch. Spanoudaki and C.S. Levin, Phys.Med.Biol. 56, 735-756 (2011);
N. Ghal-Eh, Rad.Phys.Chem. 80, 365 (2011).

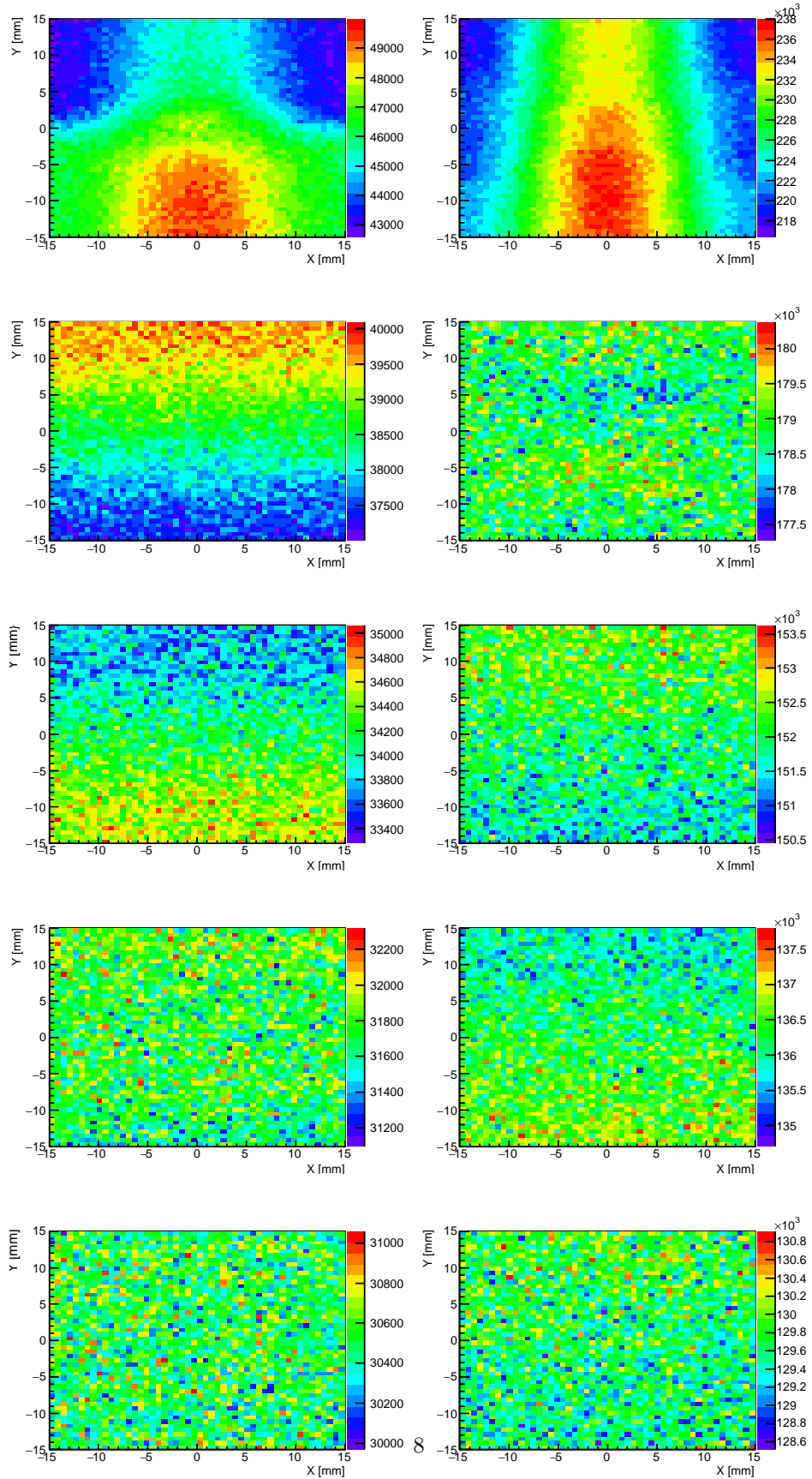


Figure 2: XY plot for optical photons that reached the photodetector side of the polished CsI (left column) and BaF₂ (right column) crystals with diffuse wrapping. Cosmic muons impinge perpendicularly to lateral side at a distance from the photodetector side of $l = 2, 6, 10, 14,$ and 18 cm (rows from top to bottom) in $-Y$ direction.

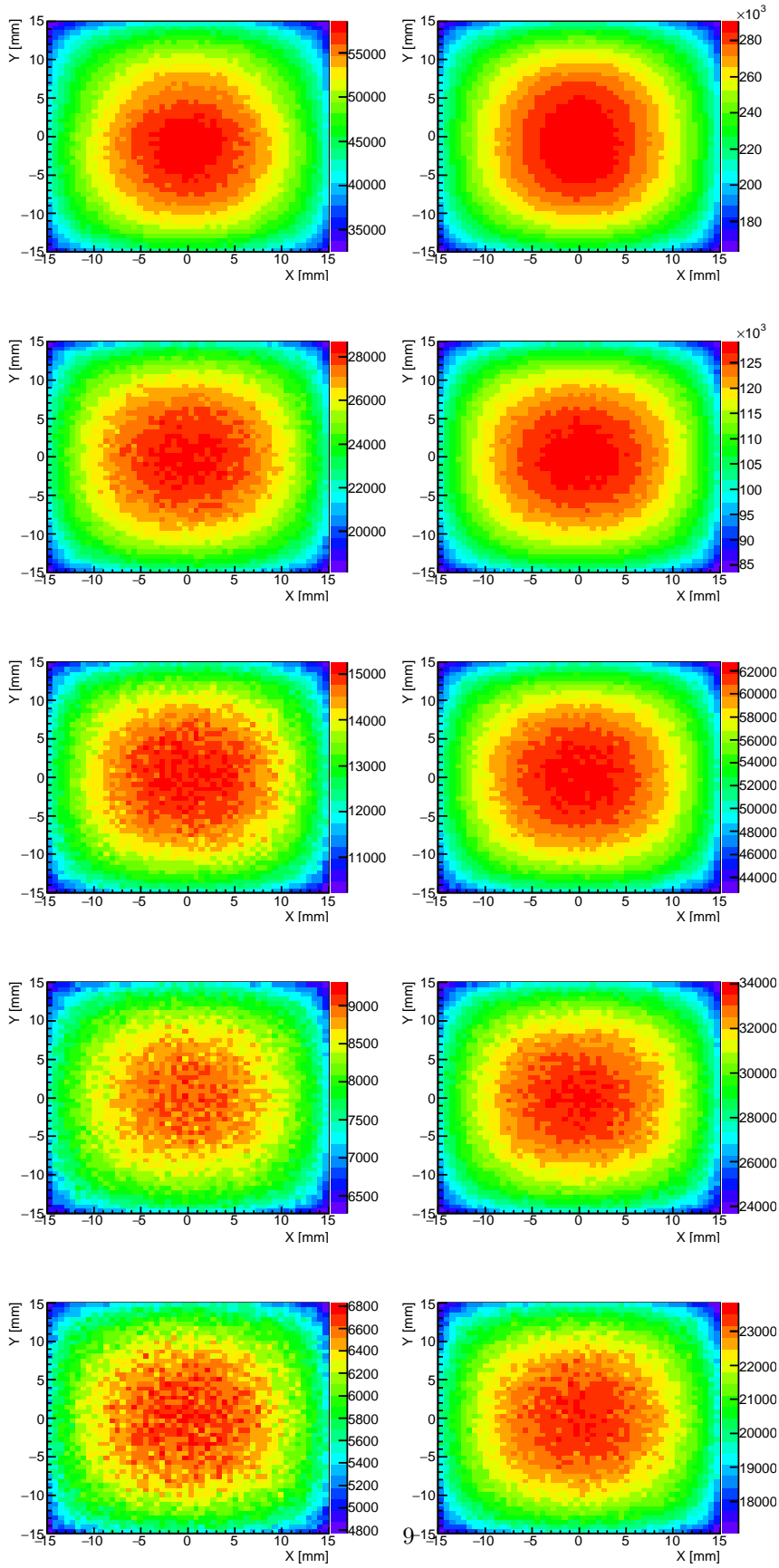


Figure 3: Same as in Figure 1, but for the ground crystal surfaces.

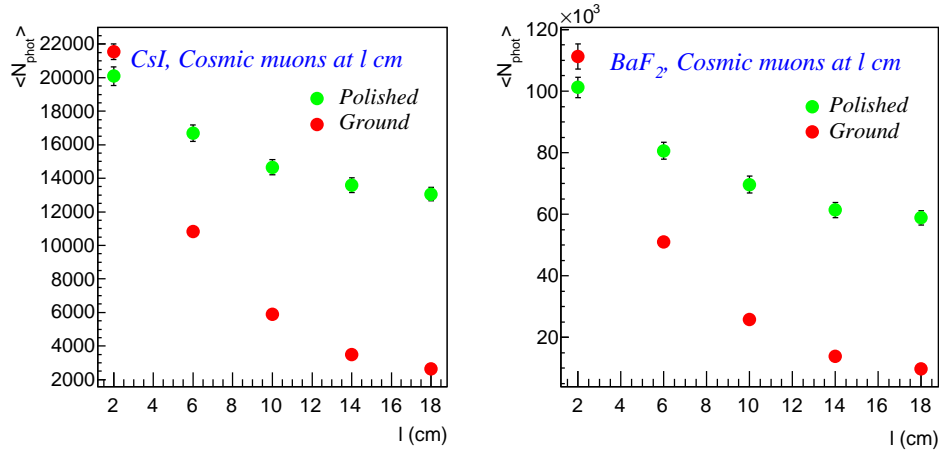


Figure 4: The mean value of the Gaussian fit of the number of optical photons arriving at the photodetector side of the CsI (left panel) and BaF₂ (right panel) crystals as a function of the distance from the cosmic muon impinging point.

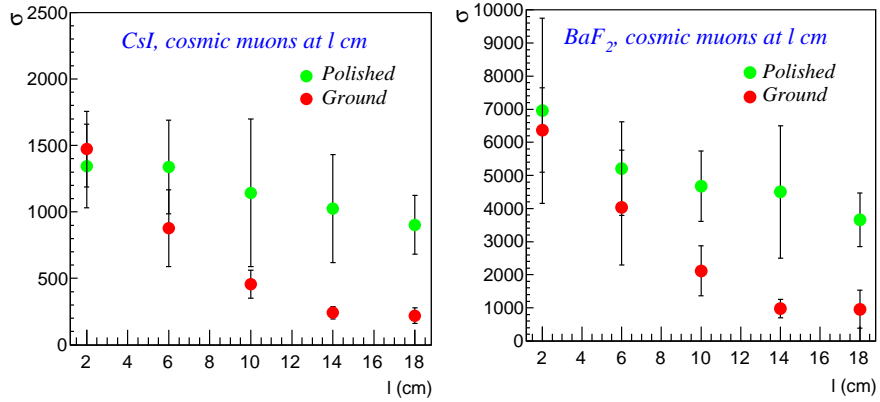


Figure 5: The standard deviation of the Gaussian fit of the number of optical photons arriving at the photodetector side of CsI (left panel) and BaF₂ (right panel) crystals as a function of the distance from the cosmic muon impinging point.

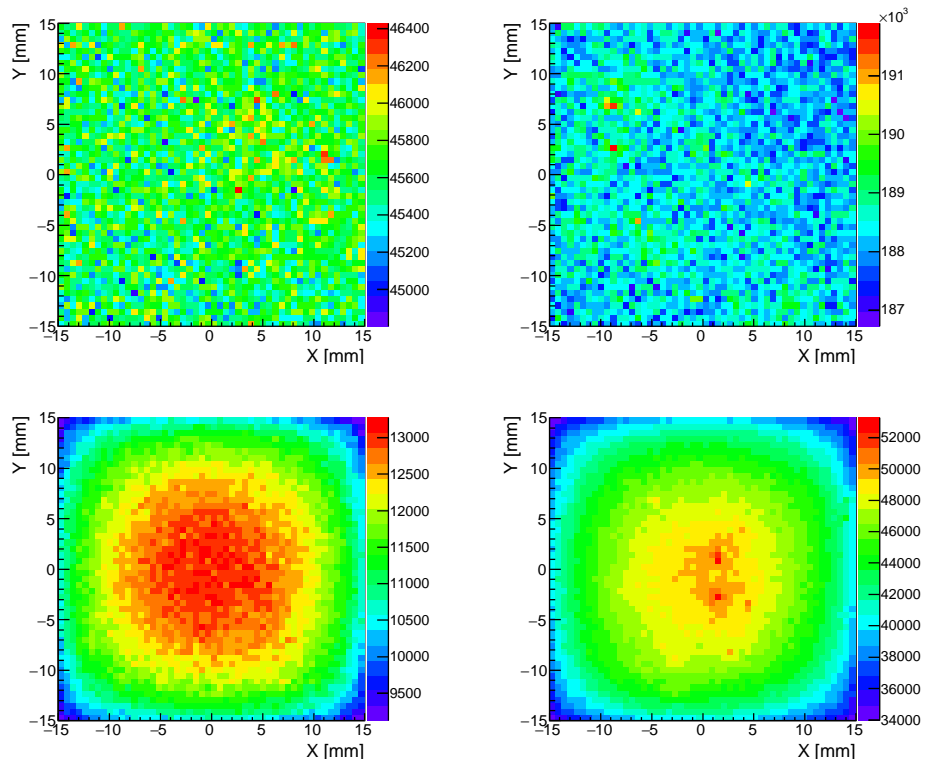


Figure 6: XY plot for the optical photons that reached the photodetector side of the CsI (left column) and BaF₂ (right column) crystals, polished (top row) and ground (bottom row). The E=105 MeV electrons impinge on the center of the opposite side of the crystal perpendicularly.

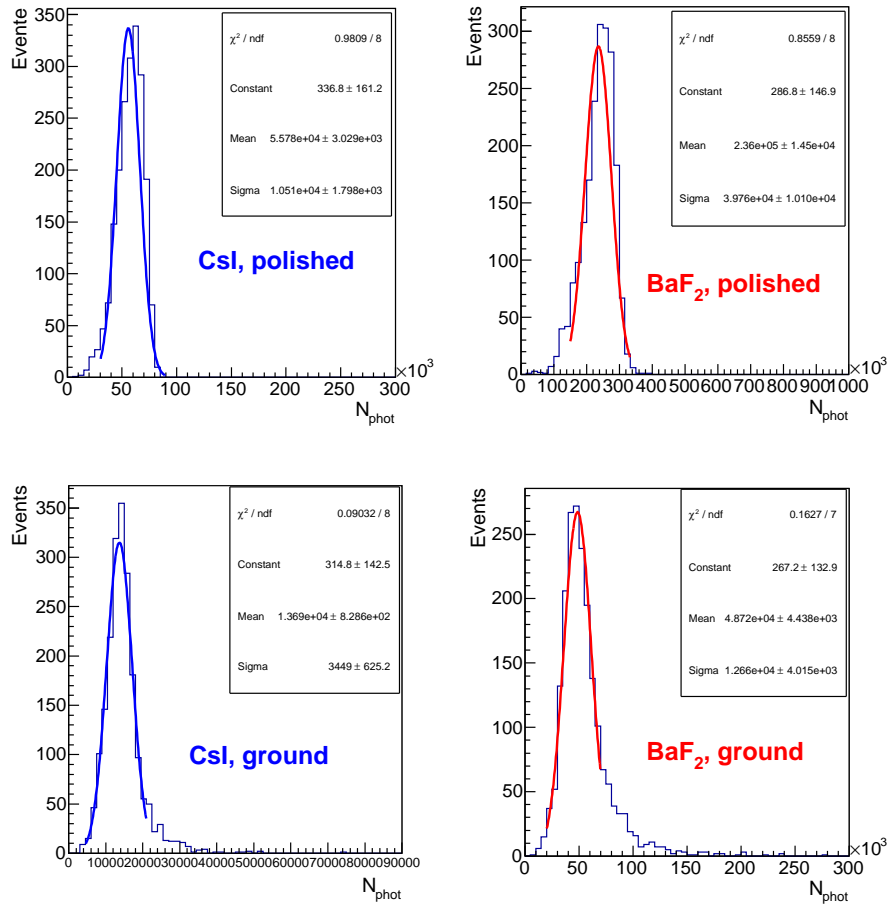


Figure 7: The optical photon number distributions corresponding to the case shown in Figure 6.

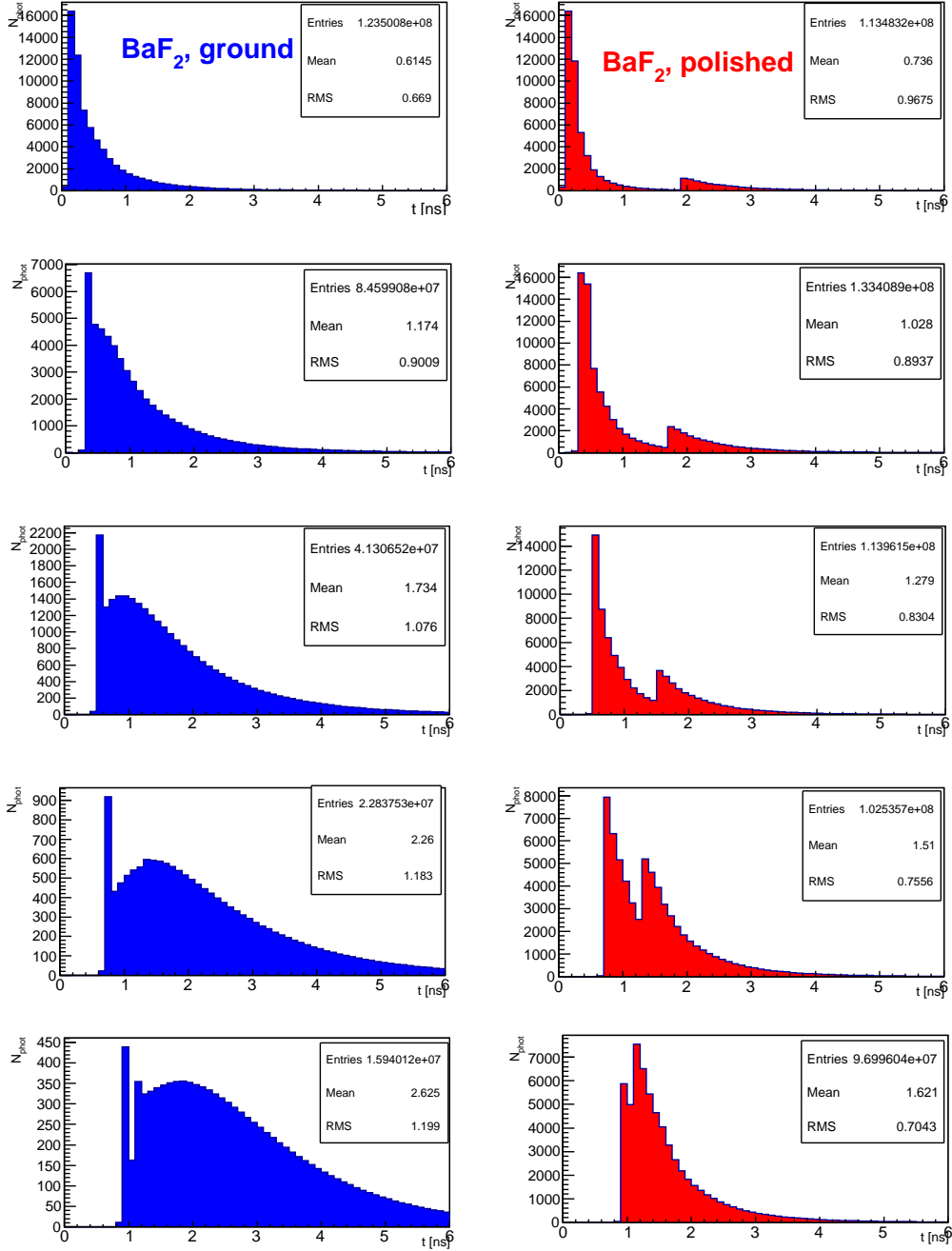


Figure 8: Optical photon arrival time at the photodetector side of the polished (right column) and ground (left column) BaF_2 crystals. Cosmic muons impinge perpendicularly to the lateral side at a distance of $l = 2, 6, 10, 14,$ and 18 cm (rows from top to bottom) from the photodetector side in $-Y$ direction.

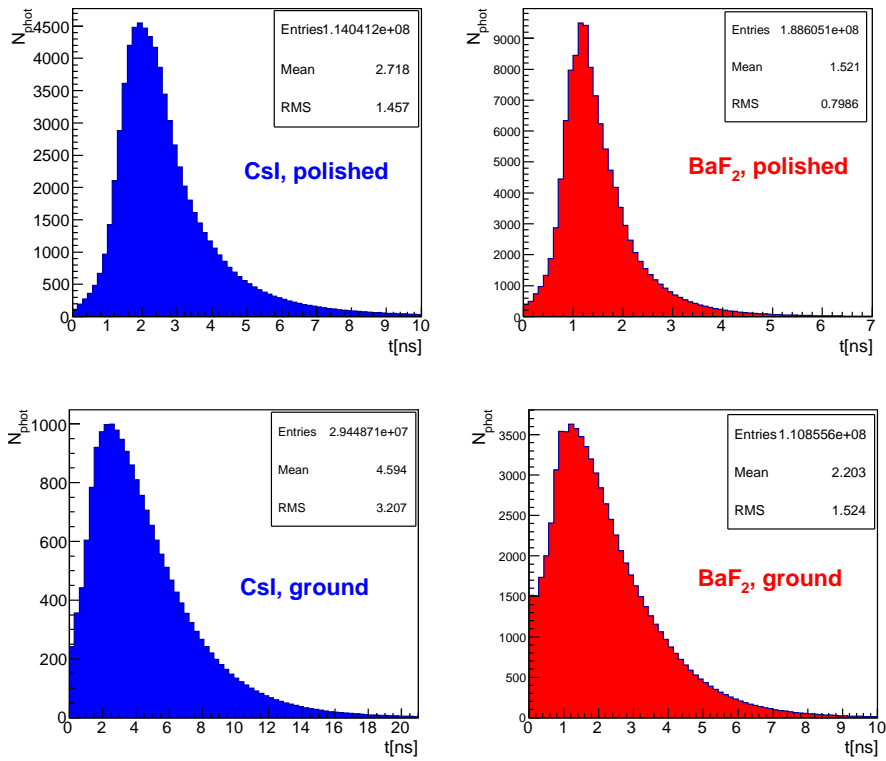


Figure 9: Optical photon arrival time at the photodetector side of the CsI (left column) and BaF₂ (right column) crystals. The crystal surfaces are polished (top row) or ground (bottom row). Electrons with $E=105$ MeV impinge on the center of the opposite side perpendicularly.

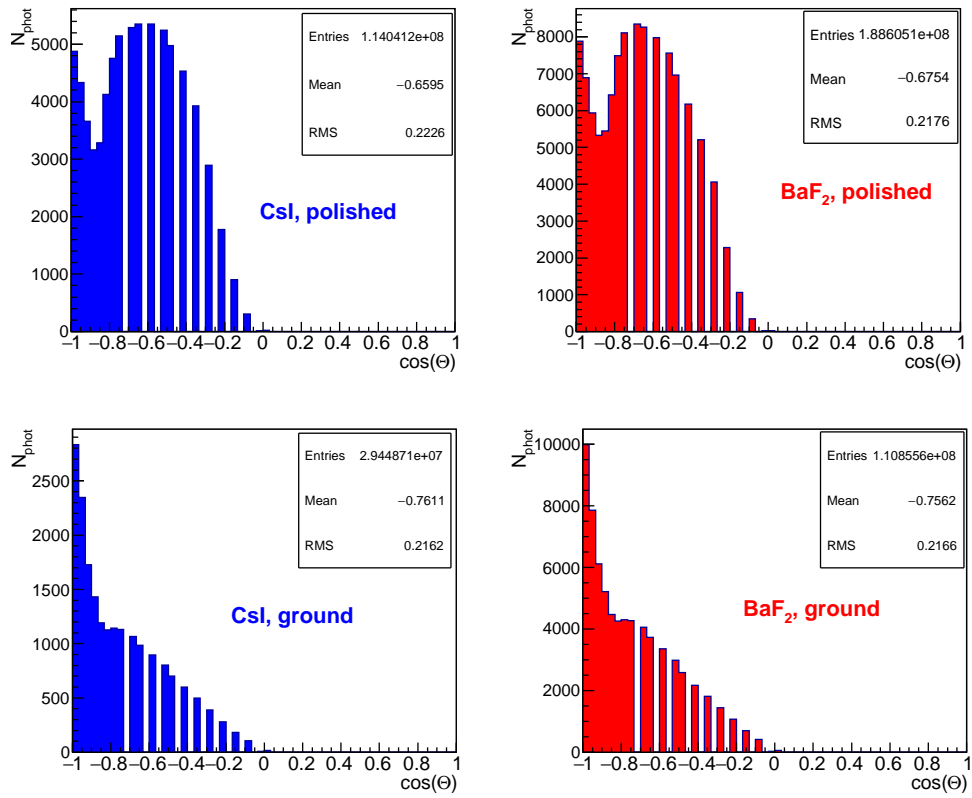


Figure 10: Incidence angle distribution of the optical photons on the photodetector side of the CsI (left column) and BaF₂ (right column) crystals. The crystal surfaces are polished (top row) or ground (bottom row). Electrons with $E=105$ MeV impinge on the center of the opposite side perpendicularly.